bioRxiv preprint doi: https://doi.org/10.64898/2026.06.02.729718; this version posted June 8, 2026. The copyright holder for this preprint (which was not certified by peer review) is the author/funder, who has granted bioRxiv a license to display the preprint in perpetuity. It is made available under a CC-BY 4.0 International license.

Submission type: Article

Asymmetric introgression and thermal advantage jointly drive climate-mediated lineage turnover in a mixed-ploidy reed

Lele Liu [1], Wenyi Sheng [1], Yuhui Wang [2], Lele Lin [3], Cui Wang [1,4], Huijia Song [5], Yaolin Guo [6], Weihua Guo [1]*

[1] School of Life Sciences, Shandong University, 72 Binhai Road, Qingdao 266237, China

[2] National Glycoengineering Research Center, Shandong University, 72 Binhai Road, Qingdao 266237, China

[3] Ecology and Nature Conservation Institute, Chinese Academy of Forestry, No.1 Dongxiaofu, Xiangshan Road, Haidian district, Beijing 100091, China

[4] Organismal and Evolutionary Biology Research Programme, Faculty of Biological and Environmental Sciences, University of Helsinki, Helsinki, Finland

[5] Natural History Museum of China, 126 Tianqiao South Street, Beijing 100050, China

[6] School of Renewable Natural Resources, Louisiana State University Agricultural Center, Baton Rouge, LA, 70803, USA

*** Corresponding author:** Weihua Guo (guowh@email.sdu.edu.cn)

bioRxiv preprint doi: https://doi.org/10.64898/2026.06.02.729718; this version posted June 8, 2026. The copyright holder for this preprint (which was not certified by peer review) is the author/funder, who has granted bioRxiv a license to display the preprint in perpetuity. It is made available under a CC-BY 4.0 International license.

Abstract

Species distribution forecasts commonly overlook intraspecific genetic variation, missing a potentially important mechanism of ecosystem change: climate-driven range shifts among lineages within a species' native range. Here we integrate population genomic analysis of 495 individuals, multi-site common garden experiments, and species distribution modeling based on 837 occurrence records for three major genetic lineages of the foundation grass *Phragmites australis* in China. The octoploid FEAU lineage (haplotype P) exhibits superior heat tolerance (critical temperature T_{crit} and T_{50}) and produces significantly greater total biomass in three of four common gardens compared to the cold-adapted CN lineage (tetraploid, haplotypes O/M), which occupies a climatic niche with lower annual mean temperature (Bio1) and mean temperature of the wettest quarter (Bio8). Genomic analyses further reveal bidirectional but asymmetric introgression, with admixed individuals showing a systematic bias toward FEAU ancestry. Under the high-emission scenario (SSP5-8.5) by 2070, projected highly suitable habitat for the FEAU lineage expands by 18.6%, while the CN lineage shows a smaller relative increase. By contrast, the subtropical SW lineage (haplotypes U/I) exhibits limited and stable suitable habitat. These results demonstrate that climate change interacts with intraspecific variation rooted in polyploidy, thermal tolerance, and asymmetric gene flow to drive potential lineage replacement within a native range, a process already suggested by field observations of FEAU expansion in a plateau lake. Our findings argue for integrating evolutionary history and genetic identity into ecological forecasting to better anticipate ecosystem responses under ongoing climate warming.

Keywords: cryptic invasion; intraspecific variation; polyploidy; climate change; foundational species.

bioRxiv preprint doi: https://doi.org/10.64898/2026.06.02.729718; this version posted June 8, 2026. The copyright holder for this preprint (which was not certified by peer review) is the author/funder, who has granted bioRxiv a license to display the preprint in perpetuity. It is made available under a CC-BY 4.0 International license.

1 Introduction

Anthropogenic climate warming is driving rapid shifts in species distributions and ecosystem composition globally, fundamentally reorganizing biodiversity (Brodie et al., 2025; Lawlor et al., 2024; Zhang et al., 2024). While species distribution models (SDMs) remain indispensable for forecasting these ecological responses, they overwhelmingly treat species as monolithic, genetically homogeneous entities (Chardon et al., 2020; Qiu et al., 2024). This assumption critically overlooks intraspecific genetic diversity, which is increasingly recognized as a primary determinant of a species adaptive capacity and vulnerability to environmental change (Cheng et al., 2021; Exposito-Alonso et al., 2022; López-Jurado et al., 2019). This knowledge gap is particularly concerning for foundation species, which disproportionately modulate community structure, habitat provision, and biogeochemical cycles (DuBois et al., 2022; Qiao et al., 2021). Consequently, ignoring their intraspecific dynamics risks missing a cryptic but profound mechanism of ecosystem reorganization: climate-driven range shifts and lineage replacement within a species native range.

The common reed, *Phragmites australis*, provides a powerful model to investigate how intraspecific variation shapes responses to global change (Eller et al., 2017; Meyerson et al., 2016). *Phragmites australis* is generally considered an allotetraploid, and hexaploids are of allopolyploid origin, whereas octoploids in Asia are most likely autopolyploid (Liu et al., 2022; Wang et al., 2024). As a nearly ubiquitous wetland foundation species, it harbors remarkable genetic and phenotypic diversity, deeply shaped by its complex evolutionary history and multiple polyploidization events (Meyerson et al., 2025; Saltonstall, 2002; Tanaka et al., 2017; Wang et al., 2024). The introduced populations of *P. australis* from Europe have shown an aggressive expansion capacity in North America (Guo et al., 2013; Saltonstall, 2002), due to smaller

bioRxiv preprint doi: https://doi.org/10.64898/2026.06.02.729718; this version posted June 8, 2026. The copyright holder for this preprint (which was not certified by peer review) is the author/funder, who has granted bioRxiv a license to display the preprint in perpetuity. It is made available under a CC-BY 4.0 International license.

64 genome size (Pyšek et al., 2018) and greater B chromosome expansion (Wang et al., 2024; Wang
65 et al., 2026). Similar lineage-specific dynamics may be unfolding within its native range in
66 China, where multiple ploidy levels coexist across distinct geographic regions.

67 In China, which is a recognized hotspot for *P. australis* genetic diversity, three major
68 genetic lineages occupying distinct geographic regions have been identified: the cold-adapted
69 CN lineage (possessing O or M haplotypes) across northern China, the FEAU lineage
70 (possessing the P haplotype, predominantly octoploid) in eastern and southern China, and the
71 SW lineage (possessing U or I haplotypes) restricted to the subtropical southwest (Liu et al.,
72 2022). This correspondence between genetic identity and ploidy level, initially suggested by the
73 geographical overlap of chloroplast haplotypes (An et al., 2012) and chromosome
74 counting-based ploidy level (C. Chen et al., 1993), has since been well established by flow
75 cytometry (Lambertini et al., 2020), allelic number comparisons from microsatellites (Liu et al.,
76 2022), and the alternative allele frequencies of reads mapped to the reference genome (Wang et
77 al., 2024).

78 The evolutionary legacy of whole-genome duplication, resulting in polyploidy, like in the
79 FEAU lineage, represents a fundamental source of its divergent adaptive potential (Cheng et al.,
80 2021; Kolář et al., 2017). Polyploidy can generate genetic novelty, alter gene expression, and
81 significantly enhance physiological stress tolerance (Bureš et al., 2024; Van de Peer et al., 2017),
82 potentially pre-equipping specific lineages to occupy new geographical range and endure
83 environmental shifts (Cheng et al., 2021; López-Jurado et al., 2019). Specifically, transcriptomic
84 and ecophysiological evidence suggests that the octoploid FEAU lineage possesses large
85 morphological traits (K. Chen et al., 1993; Guo et al., 2025; Liu et al., 2021b, 2026; Yin et al.,
86 2024), stronger salt tolerance and higher thermal tolerance in transcriptome (Wang et al., 2021)

bioRxiv preprint doi: https://doi.org/10.64898/2026.06.02.729718; this version posted June 8, 2026. The copyright holder for this preprint (which was not certified by peer review) is the author/funder, who has granted bioRxiv a license to display the preprint in perpetuity. It is made available under a CC-BY 4.0 International license.

than its tetraploid relatives. Over the past decade, FEAU lineage of *P. australis* has expanded to Caohai Lake, a plateau lake historically not occupied by this species in China (Li et al., 2026; Ran et al., 2025). Previous work suggested asymmetric introgression between the CN and FEAU lineages, but the limited number of microsatellite markers, uneven geographic sampling, and lack of dosage correction for polyploids left its direction, magnitude, and role in climate-driven expansion insufficiently resolved (Liu et al., 2022).

However, a critical question remains: how will the intraspecific differences translate into spatial biogeographic dynamics under rapid climate change? Addressing this question is essential for revealing a subtle yet potent ecological process, climate-driven lineage turnover. This process of intraspecific niche replacement represents a dynamic analogous to biological invasions but operates entirely within the native range (Paudel et al., 2025; Zhao et al., 2024).

Here, we integrate population genomics, multi-site common garden experiments, and species distribution modeling to systematically investigate how historical evolutionary legacies shape climate responses among the major genetic lineages of *P. australis* in China. We explicitly test the hypothesis that the octoploid FEAU lineage possesses superior thermal tolerance and growth performance, enabling significant range expansion under future warming, whereas the other lineages will exhibit limited capacity to track climatic shifts. By linking genomic identity, physiological tolerance, gene flow, and spatial forecasting, this study provides a mechanistic test of how polyploidy-mediated intraspecific variation governs future biogeographic patterns and the structural integrity of foundation species under global change.

bioRxiv preprint doi: https://doi.org/10.64898/2026.06.02.729718; this version posted June 8, 2026. The copyright holder for this preprint (which was not certified by peer review) is the author/funder, who has granted bioRxiv a license to display the preprint in perpetuity. It is made available under a CC-BY 4.0 International license.

2 Materials and Methods

2.1 Microsatellite genotyping and population genetics

We collected 495 leaf samples of *P. australis* from 22 provinces across China **(Table S1)**. Approximately 30 mg of dried leaf tissue from each sample was placed in a 2.0-ml tube with a 5-mm glass bead, flash-frozen in liquid nitrogen, and ground using a Tissuelyser II (Qiagen) at 30 Hz. Genomic DNA was isolated using the DNAsecure Plant Kit (Tiangen). DNA integrity was checked on agarose gels, and quality and quantity were measured with a NanoDrop 2000 spectrophotometer (Thermo Scientific). Based on the established nomenclature (Saltonstall, 2002), *Phragmites australis* haplotypes were identified using sequences from the cpDNA trnT-trnL and rbcL-psaI regions; we determined the haplotypes for 202 out of 495 samples in this and previous studies.

Phragmites australis is an allopolyploid lineage with a base allotetraploid genome, which justifies the common practice in previous microsatellite studies of selecting markers that amplify at most two alleles per individual for most tetraploids (Saltonstall, 2003). In Asia, the prevalent octoploids are most likely autopolyploid derivatives of the tetraploid, allowing ploidy level to be inferred from the number of alleles per locus observed in an individual (Liu et al., 2022). Hexaploid individuals, on the other hand, appear to be rare and mostly occur in contact zones between different lineages, where they likely originate from inter-lineage hybridization events (Wang et al., 2024). In the present study, the chosen microsatellite markers very rarely produced more than four alleles in a single individual **(Table S2)**; therefore all samples were consistently treated as tetraploid (i.e., four homologous copies). This empirical observation supports the expectation that tetraploids carry two allele copies per locus, while octoploids carry four copies, consistent with a likely autopolyploid origin of the Asian octoploids.

bioRxiv preprint doi: https://doi.org/10.64898/2026.06.02.729718; this version posted June 8, 2026. The copyright holder for this preprint (which was not certified by peer review) is the author/funder, who has granted bioRxiv a license to display the preprint in perpetuity. It is made available under a CC-BY 4.0 International license.

Microsatellite markers were designed with SSRMMD (Gou et al., 2020) based on the transcriptome sequencing of EU and FEAU lineages of *P. australis* (Wang et al., 2021). The minimum number of repeats was 6 and 5 for trinucleotide and tetranucleotide repeats, respectively. The 64 newly developed and 5 previous (PaGT9, PaGT11, PAGT12, PAGT12, PaGT14) (Saltonstall, 2003) microsatellite markers were tested with single PCR amplification in 16 representative samples. Five newly developed markers failed to get clear bands, and the remained 64 markers were tested in the multiplex PCR. In the multiplex PCR, six marked failed to amplify, and thirteen might have variation in primer regions among samples. Therefore, a total of 58 markers were used in the microsatellite genotyping for all samples **(Table S2)**. All 58 markers were aligned to the reference genome of *P. australis* (Wang et al., 2024) using minimap2 (Li, 2021), which revealed that five markers mapped to more than one chromosome. During genotyping, eleven markers, including four of the five multi-mapping markers, were removed because more than ten samples exhibited more than four alleles per sample at these loci. An additional five markers were discarded due to amplification failure in more than ten samples. One multi-mapping marker was retained owing to its ideal performance in downstream applications. Consequently, a total of 42 markers **(Table S2)** were selected for population genetic analysis. These markers are distributed across 18 out of the 25 chromosomes, including one B chromosome.

PCR amplicons (<300 bp) from each sample were pooled and tagged with 8 bp sample-specific barcodes via index primers. The barcoded products were combined into one pool for subsequent library construction. Libraries were prepared following the Illumina standard protocol and subjected to paired-end sequencing (2×150 bp) on an Illumina HiSeq 2500 platform, achieving a mean coverage of >5000× per SSR locus per sample. Raw reads were

bioRxiv preprint doi: https://doi.org/10.64898/2026.06.02.729718; this version posted June 8, 2026. The copyright holder for this preprint (which was not certified by peer review) is the author/funder, who has granted bioRxiv a license to display the preprint in perpetuity. It is made available under a CC-BY 4.0 International license.

quality-checked with FastQC. An in-house Perl script named "SSRSeq count" (str_count.pl, available at https://github.com/ccoo22/SSRseq_count) was employed to process high-quality reads and generate an SSR read count table (Cui et al., 2022). Briefly, paired-end reads were merged using FLASH, and the resulting reads were aligned to *P. australis* sequences where the SSR markers were located via Blastn. The script finally produced the microsatellite read count table summarizing read counts corresponding to alleles with varying repeat numbers for each locus and sample.

We performed microsatellite genotyping following the methodology established by the previous study, using the Perl script str_type.pl and its online implementation SSRSeq V1.1 (Cui et al., 2022). Genotyping was carried out based on read count tables, with allele calling using a threshold set according to ploidy to minimize allelic dropout. The approach incorporated corrections for stutter peaks based on empirical slip ratios and adjusted for amplification bias among alleles with varying repeat numbers. The final genotype outputs containing corrected allele dosages were formatted for subsequent population genetic analyses.

To delineate major evolutionary lineages, we performed principal coordinate analysis (PCoA) based on Bruvo's genetic distance, which is robust for polyploid data and captures the primary axes of genetic differentiation without imposing a population model. To further investigate admixture and introgression among lineages, we applied Bayesian clustering in STRUCTURE, which assumes Hardy–Weinberg equilibrium within clusters and estimates individual ancestry coefficients.

We performed Principal Coordinate Analysis (PCoA) based on genetic distance using the *polysat* package (Clark & Jasieniuk, 2011) in R, which is specifically designed for analyzing polyploid microsatellite data. Since allele dosages had already been estimated based on read

bioRxiv preprint doi: https://doi.org/10.64898/2026.06.02.729718; this version posted June 8, 2026. The copyright holder for this preprint (which was not certified by peer review) is the author/funder, who has granted bioRxiv a license to display the preprint in perpetuity. It is made available under a CC-BY 4.0 International license.

counts in prior steps, we did not utilize the genotype estimation functions within *polysat*. Instead, genetic distances between individuals were directly calculated using meandistance.matrix() under the default Bruvo's distance metric. The resulting distance matrix was then subjected to classical multidimensional scaling via the cmdscale() function.

Meanwhile, we employed a Bayesian clustering approach implemented in STRUCTURE v2.3.4 (Pritchard et al., 2000) to infer individual genetic ancestry. The number of clusters (K) was tested from 1 to 10, with five independent runs per K. Each run consisted of a burn-in period of 1,000,000 steps followed by 1,000,000 MCMC iterations. The optimal K value was determined using Structure Harvester (Earl & vonHoldt, 2012). For the selected K, we aligned the replicate runs with CLUMPP (Jakobsson & Rosenberg, 2007) to obtain a consensus population structure.

Following individual ancestry inference by STRUCTURE, we classified samples into three admixture groups (pure CN, pure FEAU, and mixed) using thresholds of 80% ancestry from a single component. To visualize spatial patterns, individual data were aggregated at the provincial level and displayed on a map of China using proportional pie charts. Regional distributions of CN ancestry were examined through histograms across three geographic regions. We quantified admixture levels using an index derived from ancestry coefficients ($1 - 2 \times |CN - 0.5|$), which was log-transformed for analysis. Linear mixed-effects models with Province as a random effect were used to assess relationships between admixture level and geographic coordinates (latitude and longitude).

A binomial test and a one-sample t-test were used to evaluate whether the proportion and mean of FEAU ancestry in admixed individuals were greater than 0.5, respectively. To infer the direction of introgression between the CN and FEAU lineages, we identified private alleles using

bioRxiv preprint doi: https://doi.org/10.64898/2026.06.02.729718; this version posted June 8, 2026. The copyright holder for this preprint (which was not certified by peer review) is the author/funder, who has granted bioRxiv a license to display the preprint in perpetuity. It is made available under a CC-BY 4.0 International license.

reference groups of geographically distant pure individuals. Pure CN here reference individuals were selected from northwestern China (longitude < 100°) with STRUCTURE ancestry coefficient $Q_{CN} > 0.9$ ($n = 70$). Pure FEAU reference individuals were selected from southeastern China (longitude > 115°) with $Q_{FEAU} > 0.9$ ($n = 44$). For each of the 42 microsatellite loci, allele frequencies were calculated separately for the two reference groups. A private allele was defined as an allele with frequency > 0.05 in one reference group and < 0.01 in the opposite group. For every individual, we scored the presence or absence of private alleles from each lineage. The proportion of pure individuals ($Q > 0.8$ for the respective lineage) carrying private alleles from the opposite lineage was calculated, and binomial tests were used to assess whether these proportions were significantly greater than 0.

2.2 Bioclimatic niche comparisons

We compiled the geographic distribution information of major published *P. australis* haplotypes in China (O, M, P, U, I). Based on our previous microsatellite and genomic studies as well as conventional nomenclature, we designated haplotypes O and M as the CN lineage (China), P as the FEAU lineage (East Asia and Australia), and U and I as the SW lineage (southwest China, or subtropical lineage). For samples whose haplotypes were not experimentally determined in this study, lineage assignments were inferred based on results from microsatellite-based PCoA. In total, we collected 837 records, comprising 365 CN, 431 FEAU, and 41 SW lineage individuals.

All bioclimatic factors for contemporary climate conditions (1979–2013) were downloaded from WorldClim database (Fick & Hijmans, 2017) for the niche analysis. To address multicollinearity among the bioclimatic variables available, pairwise Pearson correlations were calculated **(Figure S1)**. One variable from each pair exhibiting a correlation > 0.80 was randomly excluded. The initial selection of bioclimatic factors was based on the environmental

bioRxiv preprint doi: https://doi.org/10.64898/2026.06.02.729718; this version posted June 8, 2026. The copyright holder for this preprint (which was not certified by peer review) is the author/funder, who has granted bioRxiv a license to display the preprint in perpetuity. It is made available under a CC-BY 4.0 International license.

requirements of *P. australis* and previous species distribution model study of this species (Guo et al., 2013). The filtering yielded a final subset of eight key predictors for the niche comparison and further MaxEnt modeling: annual mean temperature (bio1), mean diurnal range (bio2), isothermality (bio3), temperature seasonality (bio4), mean temperature of wettest quarter (bio8), precipitation of driest month (bio14), precipitation seasonality (bio15), and precipitation of warmest quarter (bio18). Statistical differences in bioclimatic variables among lineages were assessed using Kruskal–Wallis tests with Benjamini–Hochberg (BH) *p*-value adjustment.

The environmental space of the CN and FEAU lineages was characterized using the "Characterize Environmental Space" component in the Wallace 2 platform (Kass et al., 2023). This module was employed to visualize and compare the Hutchinsonian niches of the two lineages. Specifically, a Principal Component Analysis (PCA) was performed using the Environmental Ordination module to reduce the dimensionality of the environmental data, followed by a niche overlap analysis conducted via the Niche Overlap module.

2.3 Common garden experiments

To investigate the growth differences and adaptive strategies between the CN and FEAU lineages, we collected growth data, including total biomass, shoot height, density, and specific leaf area (SLA), from two parallel common garden experiments: (1) A previously published common garden experiment (Song et al., 2021) conducted in 2017 across Jinnan (36.43°N, 117.45°E) and Panjin (41.20°N, 122.02°E), using CN (n = 11) and FEAU (n = 9) lineages, for which we determined the haplotype information of all samples; (2) A new common garden experiment established in 2021 across Qingdao (36.36°N, 120.69°E) and Shanghai (30.20°N, 121.29°E), with CN (n = 9) and FEAU (n = 8) lineages **(Table S3)**.

bioRxiv preprint doi: https://doi.org/10.64898/2026.06.02.729718; this version posted June 8, 2026. The copyright holder for this preprint (which was not certified by peer review) is the author/funder, who has granted bioRxiv a license to display the preprint in perpetuity. It is made available under a CC-BY 4.0 International license.

In both experiments, rhizomes were propagated hydroponically and segmented to produce 5–6 segments per population (each with 2–3 buds), which were then transplanted individually into 20 L pots containing a standardized soil substrate. Identical populations were planted simultaneously at both sites under rigorously controlled conditions, with uniform substrate, container size, fertilization, and pesticide application, thereby isolating ambient climate as the sole environmental variable. Garden management was synchronized across sites throughout the growing season, including bi-weekly irrigation (adjusted for ambient precipitation), monthly application of balanced fertilizer from June to September, and standardized pest and disease control.

Measurement protocols were consistent across both gardens. Plant height was defined as the distance from the soil surface to the tallest inflorescence or, in its absence, the highest leaf tip. For each pot, the heights of the three tallest shoots were measured and averaged. Five fully expanded leaves (from nodes 3–5) per pot were randomly selected, placed in labeled plastic bags, and rehydrated in darkness for 12 hours prior to measuring saturated fresh mass. Leaf areas were determined from scanned images using ImageJ software calibrated with a millimeter scale. All leaf samples were then oven-dried at 80 °C for 48 hours and weighed. Aboveground biomass was harvested by cutting shoots at soil level, placed in paper bags, and dried at 80 °C until constant mass was achieved. Total belowground dry mass was estimated by extrapolating the fresh-to-dry mass ratio obtained from a subsample to the entire root system.

For each trait separately, we calculated the mean and standard error (SE) for each lineage within each garden. To assess the statistical significance of differences between the two lineages within each garden, pairwise Student's *t*-tests were performed independently for each garden-trait

bioRxiv preprint doi: https://doi.org/10.64898/2026.06.02.729718; this version posted June 8, 2026. The copyright holder for this preprint (which was not certified by peer review) is the author/funder, who has granted bioRxiv a license to display the preprint in perpetuity. It is made available under a CC-BY 4.0 International license.

266 combination. No correction for multiple testing was applied, as each common garden was
267 considered an independent experimental environment.

268 **2.4 Heat tolerance measurement**

269 Heat tolerance was assessed on a sunny morning after approximately three months of cultivation.
270 For each of the 12 *P. australis* genotypes (6 FEAU and 6 CN) grown in a common garden
271 (36.38°N, 118.90°E) located in Weifang, Shandong Province, China in 2024, the third or fourth
272 fully expanded leaves were selected. After excision, the leaves were wrapped in moist tissue
273 paper, placed in ziplock bags with ice packs, and transported to the laboratory under dark
274 conditions to minimize transpiration. In the laboratory, the leaves were cut into segments
275 approximately 1 cm in length. These segments were then wrapped in wet filter paper, sealed in
276 plastic bags, and subjected to heat treatment in a water bath. The temperature regimen consisted
277 of sequential exposure to 25 ℃ (ambient control), 38 ℃, 40 ℃, 42 ℃, 44 ℃, 46 ℃, 48 ℃,
278 50 ℃, 52 ℃, 54 ℃, 57 ℃, and 60 ℃. Following heat treatment, all samples were kept in moist,
279 dark conditions for 24 hours. After dark adaptation, the maximum quantum yield of photosystem
280 II (Fv/Fm) was measured using a pulse-amplitude modulation (PAM) fluorometer (PAM-2500,
281 Walz, Effeltrich, Germany). Each temperature treatment included five biological replicates.

282 Parameters of heat tolerance (T_{crit}, T_{50}, and T_{95}) were derived from a logistic decay model
283 that describes the relationship between Fv/Fm and temperature. Parameter estimates were
284 obtained through nonlinear least-squares regression using the *nls* routine in R. Mean values for
285 each parameter were calculated using bootstrap resampling, implemented within a custom R
286 function (psiiht), which also provided optional diagnostic plotting (Perez et al., 2021). The
287 critical temperature (T_{crit}) was identified as the temperature at which the slope of the Fv/Fm
288 decline reached 15% of the maximum negative slope observed during heating, with the

bioRxiv preprint doi: https://doi.org/10.64898/2026.06.02.729718; this version posted June 8, 2026. The copyright holder for this preprint (which was not certified by peer review) is the author/funder, who has granted bioRxiv a license to display the preprint in perpetuity. It is made available under a CC-BY 4.0 International license.

additional constraint that this point must occur below the temperature causing 50% inhibition. The temperature of 50% inhibition (T_{50}) was defined as the point at which Fv/Fm decreased to half of the value measured at the control temperature. Similarly, the temperature of 95% inhibition (T_{95}) corresponds to a 95% reduction in Fv/Fm relative to the control level. All three parameters were compared between CN and FEAU lineages using a *t*-test.

2.5 Species distribution models

To assess the impact of climatic changes on the distribution of *P. australis* lineages, species distribution models were developed using eight selected bioclimatic variables. Potential geographic distributions were projected using the maximum entropy algorithm (MaxEnt) within Wallace (Kass et al., 2023). MaxEnt models species distributions by comparing environmental conditions at occurrence sites with those across the background environment. The model was calibrated with 10,000 randomly generated background points from the study region. Regularization multipliers were tested ranging from 0.5 to 5.0 at intervals of 0.5, and all feature class combinations (Linear, Quadratic, Hinge, Product) were examined. Model selection followed a random k-fold cross-validation approach ($k = 4$), with the best model chosen based on the lowest corrected Akaike Information Criterion (ΔAICc).

For projecting future distributions across both native and introduced ranges, bioclimatic variables at 5-arcmin resolution were obtained from WorldClim. Future projections for the period 2061–2080 incorporated two representative climate scenarios: the low-emission pathway SSP1-2.6 and the high-emission pathway SSP5-8.5 (IPCC, 2021). Future climate projections were derived from the Centre National de Recherches Météorologiques Earth System Model 2-1 (CNRM-ESM2-1) (Séférian et al., 2019).

bioRxiv preprint doi: https://doi.org/10.64898/2026.06.02.729718; this version posted June 8, 2026. The copyright holder for this preprint (which was not certified by peer review) is the author/funder, who has granted bioRxiv a license to display the preprint in perpetuity. It is made available under a CC-BY 4.0 International license.

3 Results

3.1 Genetic structure and lineage delimitation

Given that STRUCTURE showed optimal $K = 2$ **(Figure S2)** and failed to fully resolve the SW lineage **(Figure 1A)**, we used PCoA for lineage delineation **(Figure 1B)** and STRUCTURE for admixture quantification **(Figure 2)**. This complementary approach allows us to distinguish between evolutionary lineage identity and contemporary gene flow.

The PCoA clearly resolved three major genetic clusters, along with a few introgressive and nuclear-chloroplast discordant samples **(Figure 1B)**. Coordinate 1, explaining 22.05% of the variance, separated the FEAU lineage (haplotype P and related haplotypes such as AS) from the CN lineage (haplotypes O and M). Coordinate 2, which explained 9.36% of the variance, distinguished the SW lineage (haplotypes U and I).

For the Bayesian clustering analysis in STRUCTURE, at $K = 2$, two genetic clusters were identified, distributed across northern and southern China, respectively **(Figure 1A)**, corresponding to the previously reported CN and FEAU lineage. When K was increased to 3, a southwestern genetic component was further differentiated **(Figure S3)**.

Admixture between CN and FEAU lineages was widespread across China, with a general predominance of FEAU ancestry **(Figure 2A)**. The spatial distribution of admixture groups, however, exhibited distinct regional patterns **(Figure 2B–E)**. Southern China was predominantly occupied by pure FEAU and mixed individuals, northwestern China was dominated by pure CN with a limited presence of mixed types, while northern China was primarily characterized by admixed individuals alongside both pure FEAU and CN lineages **(Figure 2B, C)**. These

bioRxiv preprint doi: https://doi.org/10.64898/2026.06.02.729718; this version posted June 8, 2026. The copyright holder for this preprint (which was not certified by peer review) is the author/funder, who has granted bioRxiv a license to display the preprint in perpetuity. It is made available under a CC-BY 4.0 International license.

geographical gradients resulted in a significant longitudinal effect on admixture levels (p = 0.013), whereas no significant latitudinal pattern was observed (p = 0.873) **(Figure 2D, E)**.

Among the 131 individuals classified as admixed (Q_{CN} and Q_{FEAU} both between 0.2 and 0.8), 80 individuals (61.1%) had a FEAU ancestry proportion greater than 0.5 (0.569 ± 0.16). Both the proportion (binomial test, p = 0.007) and the mean (one-sample t-test, t = 4.89, df = 130, $p < 0.001$) were significantly greater than 0.5, indicating a systematic bias toward FEAU ancestry in admixed individuals. Using reference groups of 70 pure CN individuals and 44 pure FEAU individuals, we identified 16 CN-private alleles and 19 FEAU-private alleles across the 42 microsatellite loci. Among 194 pure CN individuals ($Q_{CN} > 0.8$), 56 individuals (28.9%) carried at least one FEAU-private allele (binomial test, $p < 0.001$). Among 168 pure FEAU individuals ($Q_{FEAU} > 0.8$), 77 individuals (45.8%) carried at least one CN-private allele ($p <$ 0.001). These results demonstrate bidirectional gene flow between the two lineages, with CN → FEAU introgression being more prevalent at the level of private alleles.

3.2 Differentiation of bioclimatic niche among lineages

Significant differences were observed among lineages across all eight bioclimatic variables analyzed **(Figure 1C)**. For bio1, bio3, bio8, and bio18, the FEAU lineage exhibited values significantly higher than those of CN but lower than those of SW. In contrast, for bio2 and bio4, values in FEAU were significantly lower than in CN but higher than in SW. Meanwhile, CN showed significantly lower values than both FEAU and SW in bio14, but higher values in bio15 **(Figure 1D)**.

Following environmental PCA **(Figure S4)**, niche similarity tests revealed a statistically significant moderate overlap between the CN and FEAU lineages **(Figure S5)** (Schoener's D = 0.48, p = 0.01). Specifically, 16% of the environmental space was occupied exclusively by the

bioRxiv preprint doi: https://doi.org/10.64898/2026.06.02.729718; this version posted June 8, 2026. The copyright holder for this preprint (which was not certified by peer review) is the author/funder, who has granted bioRxiv a license to display the preprint in perpetuity. It is made available under a CC-BY 4.0 International license.

CN lineage, while 40% was unique to the FEAU lineage. Approximately 60% of the environmental space was shared by both lineages, indicating considerable common habitat suitability despite their distinct ecological characteristics.

3.3 Differentiation of growth performance between two lineages

The four common gardens are all located in eastern China where the CN and FEAU lineages co-occur, with mean annual temperature (Bio1) ranging from 9.3 ℃ (Panjin) to 16.8 ℃ (Shanghai) **(Figure 3A)**. The total biomass of the FEAU lineage was significantly greater than that of the CN lineage in Jinan, Panjin, and Qingdao, but no significant difference was observed in Shanghai **(Figure 3B)**. Similarly, plant height was significantly greater in the FEAU lineage than in the CN lineage in Jinan, but not in the other common gardens (**Figure 3C**). In contrast, the CN lineage exhibited significantly higher density than the FEAU lineage in Jinan and Panjin, while no significant differences were detected in Qingdao or Shanghai (**Figure 3D**). For specific leaf area (SLA), no significant differences were found between the two lineages in any of the common gardens (**Figure 3E**).

3.4 Heat tolerance of two lineages

The heat tolerance parameters T_{crit}, T_{50}, and T_{95} were compared between CN and FEAU lineages (**Figure 3F**; **Figure S6; Table S4)**. The mean T_{crit} for the CN group was 42.9 ± 1.04 ℃, which was significantly lower than that of the FEAU group (44.2 ± 0.96 ℃; $p < 0.05$). Similarly, a significant difference was observed in T_{50}, with the CN group exhibiting a mean of 47.7 ± 0.56 ℃ compared to 48.5 ± 0.78 ℃ in the FEAU group ($p < 0.05$). In contrast, no significant

bioRxiv preprint doi: https://doi.org/10.64898/2026.06.02.729718; this version posted June 8, 2026. The copyright holder for this preprint (which was not certified by peer review) is the author/funder, who has granted bioRxiv a license to display the preprint in perpetuity. It is made available under a CC-BY 4.0 International license.

difference was detected in T_{95} between the two groups; the mean values were 51.6 ± 0.83 ℃ for CN and 52.1 ± 1.36 ℃ for FEAU.

3.5. Potential distribution projection of three lineages

The optimal model configurations and performance metrics varied among the three lineages **(Table S5)**. The CN lineage achieved the best fit with the LQHP feature class and a regularization multiplier of 0.5, resulting in high predictive accuracy (AUCtrain = 0.947) and excellent model stability (CBItrain = 0.973). This model was strongly supported (AICc weight ≈ 1.000). The FEAU lineage performed best under the LQH feature class and RM = 0.5, also showing high training AUC (0.946) and good validation performance (AUCval = 0.898). In contrast, the SW lineage was best modelled using a simpler LQ feature class with RM = 1.0, yielding the highest training AUC (0.965) but lower complexity (7 coefficients). All models demonstrated high predictive performance, with training AUC values exceeding 0.94.

Model projections indicated notable shifts in habitat suitability under future climate scenarios **(Figure 4; Figure S7; Table S6)**. For the CN lineage, the high-emission scenario (SSP5-8.5) resulted in a marked expansion of high-suitability areas to 16.5%, compared to 9.4% under current conditions. In contrast, the FEAU lineage showed the most pronounced response under SSP5-8.5, with high-suitability habitat increasing substantially to 25.2%, while low-suitability areas contracted to 56.7%. The SW lineage remained relatively stable across projections, with the majority of habitats consistently classified as low suitability, though a slight increase in high and medium suitability was observed under SSP5-8.5. These results suggest

bioRxiv preprint doi: https://doi.org/10.64898/2026.06.02.729718; this version posted June 8, 2026. The copyright holder for this preprint (which was not certified by peer review) is the author/funder, who has granted bioRxiv a license to display the preprint in perpetuity. It is made available under a CC-BY 4.0 International license.

395 divergent responses to climate change among lineages, with FEAU exhibiting the greatest
396 potential for range expansion under high-emission scenarios.

397 **4 Discussion**

398 **4.1 Ecophysiological basis of thermal tolerance and range expansion**

399 Our findings demonstrate that the octoploid FEAU lineage of *P. australis* possesses greater heat
400 tolerance and biomass production than the tetraploid CN lineage. Under a high emission scenario
401 (SSP5 8.5), the projected suitable habitat for the FEAU lineage expands by 18.6%, while the CN
402 lineage exhibits a much smaller relative increase. These results support the hypothesis that
403 polyploidy can confer physiological advantages that translate into asymmetric range dynamics
404 within a species' native range (Bureš et al., 2024; Van de Peer et al., 2017).

405 The superior heat tolerance of the FEAU lineage, characterized by an approximately 1.3 ℃
406 higher T_{crit} and 0.8 ℃ higher T_{50}, aligns with evidence that whole genome duplication can
407 enhance stress tolerance through gene dosage effects, subfunctionalization, or epigenetic
408 modifications (Van de Peer et al., 2017). In *P. australis*, transcriptomic comparisons have
409 revealed that octoploids upregulate heat shock proteins and maintain photosystem II integrity
410 under elevated temperatures (Wang et al., 2021). Similar patterns occur in other polyploid
411 systems, such as *Dianthus broteri* (López-Jurado et al., 2019) and *Fragaria* (Wei et al., 2020),
412 although this advantage can be context dependent (Kolář et al., 2017).

413 A 1.3 ℃ difference in T_{crit} could be critical when summer temperatures approach or exceed
414 a lineage's photosynthetic thermal thresholds. Mean annual air temperature over China has risen
415 by more than 1 ℃, with more frequent and hotter summer days (Wei et al., 2023). In eastern
416 China, extreme heat events are becoming more frequent and intense, with peak summer
417 temperatures increasingly approaching the critical thresholds (42.9 ℃ for CN, 44.2 ℃ for

bioRxiv preprint doi: https://doi.org/10.64898/2026.06.02.729718; this version posted June 8, 2026. The copyright holder for this preprint (which was not certified by peer review) is the author/funder, who has granted bioRxiv a license to display the preprint in perpetuity. It is made available under a CC-BY 4.0 International license.

418 FEAU) identified here (Zhou et al., 2024). Direct evidence linking PSII heat tolerance to survival
419 in wetland plants remains limited (Perez et al., 2021), yet the functional consequence is clear: a
420 lineage that maintains photosynthesis at 44 ℃ rather than ceasing at 43 ℃ will sustain carbon
421 assimilation longer during heatwaves. Unlike woody plants in drylands, where heatwave
422 mortality often results from hydraulic failure (Breshears et al., 2021), *P. australis* in wetlands is
423 unlikely to face severe water limitation; direct thermal damage to the photosynthetic apparatus is
424 the primary constraint. Even marginal differences in thermal tolerance can be amplified through
425 positive feedback: prolonged carbon assimilation leads to greater biomass, which in turn
426 enhances competitive ability and accelerates range expansion (Cheng et al., 2021). Therefore, the
427 consistent physiological differences documented here are likely to translate into meaningful
428 demographic advantages under the intensifying heat regimes expected across eastern China.

429 **4.2 Niche overlap, admixture, and the trajectory of lineage replacement**

430 Bayesian clustering and principal coordinate analysis resolved three distinct genetic lineages,
431 revealing a broad zone of admixture between the FEAU and CN lineages in northern China. A
432 substantial proportion of individuals exhibited mixed ancestry, with admixture levels increasing
433 significantly with longitude but not latitude, consistent with a previous study using limited
434 microsatellite markers (Liu et al., 2022). This east–west gradient suggests ongoing gene flow,
435 which may be facilitated by both natural and human-mediated dispersal. Eastward water
436 dispersal via the Yellow River (Liu et al., 2021a, 2021b) and historical introductions of *P.*
437 *australis* germplasm for reed production in areas such as the Panjin region (Brix et al., 2014)
438 likely contribute to this pattern. However, the persistence of pure CN and pure FEAU individuals
439 within admixed populations implies that reproductive barriers or selection against hybrids exist,
440 potentially driven by ploidy differences (tetraploid versus octoploid) or local adaptation.

bioRxiv preprint doi: https://doi.org/10.64898/2026.06.02.729718; this version posted June 8, 2026. The copyright holder for this preprint (which was not certified by peer review) is the author/funder, who has granted bioRxiv a license to display the preprint in perpetuity. It is made available under a CC-BY 4.0 International license.

441 The moderate environmental niche overlap between CN and FEAU (Schoener's $D = 0.48$)
442 indicates that approximately 60% of their environmental space is shared. Under current climatic
443 conditions, parapatric coexistence and the observed admixture patterns may be maintained by
444 dispersal limitations or competitive trade-offs (Guo et al., 2024; Liu et al., 2026). For example,
445 the CN lineage's higher shoot density at northern sites may contribute to its persistence in cooler
446 regions, potentially offsetting the demographic disadvantages of its lower heat tolerance and
447 morphological size. However, coexistence theory predicts that when two lineages share a large
448 fraction of environmental space and one possesses a consistent performance advantage,
449 competitive exclusion is likely to occur in a changing environment (Pastore et al., 2021).
450 Furthermore, the octoploid FEAU lineage likely possesses greater genomic compatibility than
451 the tetraploid CN lineage, leading to asymmetric introgression: hybrids are expected to backcross
452 more frequently with the high-ploidy lineage (Bartolić et al., 2024; Han et al., 2015; Liu et al.,
453 2022; Zohren et al., 2016), gradually shifting the genetic composition of admixed populations
454 toward the FEAU genome. Supporting this hypothesis, private allele analysis revealed
455 bidirectional gene flow, with 28.9% of pure CN individuals carrying FEAU-private alleles and
456 45.8% of pure FEAU individuals carrying CN-private alleles. Crucially, admixed individuals
457 showed a significant bias toward FEAU ancestry (61.1%), consistent with asymmetric
458 backcrossing favoring the octoploid genome.
459 Our common garden results corroborate this trajectory: the FEAU lineage produced
460 significantly greater biomass than CN in three gardens (Jinan, Panjin, and Qingdao), but not in
461 the warmest (Shanghai). This exception may reflect other limiting factors in Shanghai or indicate
462 that FEAU's thermal advantage diminishes near its upper physiological limits. Because the two

bioRxiv preprint doi: https://doi.org/10.64898/2026.06.02.729718; this version posted June 8, 2026. The copyright holder for this preprint (which was not certified by peer review) is the author/funder, who has granted bioRxiv a license to display the preprint in perpetuity. It is made available under a CC-BY 4.0 International license.

463 experiments differed in starting material and growth duration, we focus only on the direction and
464 significance of lineage differences within each site, not on absolute biomass across gardens.

465 As warming progresses, the competitive balance is expected to shift decisively toward
466 FEAU. The current admixture zone may act as a moving hybrid front, with FEAU gradually
467 displacing CN in warmer regions while potentially maintaining a stable hybrid zone in
468 transitional climates. This projected lineage replacement differs fundamentally from the
469 non-native invasion of *P. australis* in North America (Saltonstall, 2002), where an introduced
470 European lineage spread into novel territory; in China, the expansion involves only native
471 genotypes. Nevertheless, both processes threaten to erode unique genetic diversity and reduce the
472 species' adaptive capacity.

473 **4.3 Vulnerability of the SW lineage and potential ecosystem consequences**

474 The SW lineage, with only 41 occurrence records and a restricted distribution, occupies a distinct
475 climatic niche and is projected to remain spatially limited under future scenarios. This stability
476 likely reflects a narrow fundamental niche rather than resilience. Field observations of FEAU
477 encroachment into Caohai Lake, a site historically not occupied by *P. australis* (Li et al., 2026;
478 Ran et al., 2025), echo patterns seen in other systems where warm adapted lineages displace cold
479 adapted ones (Cheng et al., 2021; Paudel et al., 2025). Although not yet quantified, this trend
480 merits urgent monitoring. The SW lineage should be considered a high priority conservation
481 target, and its habitats must be carefully managed to minimize the inadvertent introduction of
482 FEAU propagules (Tanaka et al., 2017).

483 The potential replacement of the CN lineage by the FEAU lineage, if realized, could have
484 ecosystem-level consequences beyond genetic composition. As a foundation species, *P.*
485 *australis* modulates wetland structure and biogeochemical cycles. The FEAU lineage's tendency

bioRxiv preprint doi: https://doi.org/10.64898/2026.06.02.729718; this version posted June 8, 2026. The copyright holder for this preprint (which was not certified by peer review) is the author/funder, who has granted bioRxiv a license to display the preprint in perpetuity. It is made available under a CC-BY 4.0 International license.

toward greater biomass but lower shoot density may alter light availability, sediment dynamics, and habitat complexity for invertebrates (Yan et al., 2021). However, these ecosystem consequences remain speculative. Direct measurements of decomposition rates, greenhouse gas fluxes, and faunal communities across monospecific stands of each lineage are required to test these hypotheses.

4.4 Limitations, future directions, and conservation implications

While our SDM projections provide a robust framework for assessing vulnerability, they inherently assume unlimited dispersal and an absence of novel biotic interactions (Di Cola et al., 2017; Phillips et al., 2017). The natural expansion of the FEAU lineage will ultimately depend on propagule dispersal distances (seeds and rhizomes) and landscape barriers (Liu et al., 2021a). The current admixture zone in northern China confirms that gene flow is active, but the actual rate of spread may lag model projections. Future work should integrate mechanistic dispersal models and long-term field monitoring of contact zones to validate these spatial predictions. Moreover, precipitation changes and land use conversion were not fully accounted for, both of which could alter habitat suitability across regions (Guo et al., 2013).

Additionally, although polyploidy is strongly implicated in underpinning the FEAU lineage's thermal advantage, ploidy was not experimentally manipulated in this study. Future common garden experiments utilizing near isogenic lines of different ploidies, or transcriptomic analyses that explicitly partition ploidy effects from lineage effects, are needed to strengthen causal inference (Wei et al., 2020). The potential role of admixture in facilitating the adaptive introgression of heat tolerance alleles also warrants deeper investigation (Suarez-Gonzalez et al., 2018).

bioRxiv preprint doi: https://doi.org/10.64898/2026.06.02.729718; this version posted June 8, 2026. The copyright holder for this preprint (which was not certified by peer review) is the author/funder, who has granted bioRxiv a license to display the preprint in perpetuity. It is made available under a CC-BY 4.0 International license.

The projected replacement of a cold adapted native lineage by a warm adapted native lineage presents a nuanced conservation challenge. Unlike classical biological invasions, no non-native species is involved; nevertheless, the loss of unique regional gene pools (CN and SW) may erode the species' overall adaptive capacity to future environmental volatility (Exposito-Alonso et al., 2022). To safeguard evolutionary resilience, we recommend three practical measures: using strictly locally sourced germplasm in wetland restoration to prevent the human mediated spread of the FEAU lineage; protecting established hybrid zones as reservoirs of genetic diversity; and establishing long-term monitoring networks in geographic contact zones to detect lineage turnover early (Brodie et al., 2025; Lawlor et al., 2024; Vranken et al., 2021).

Conclusions

The integration of population genomics, common garden experiments, and species distribution modeling reveals three interacting mechanisms that jointly drive lineage turnover under climate warming. First, the octoploid FEAU lineage possesses superior thermal tolerance (1.3 ℃ higher T_{crit}) compared to the tetraploid CN lineage. Second, the octoploid lineage exhibits intrinsically greater biomass production, a trait that is likely an inherent consequence of polyploidy and further reinforced by its thermal tolerance, together enhancing its competitive ability. Third, asymmetric introgression, resulting from preferential backcrossing of hybrids with the octoploid FEAU lineage, progressively shifts the genomic composition of admixed populations toward FEAU. These mechanisms, coupled with moderate niche overlap and ongoing gene flow, strongly suggest a trajectory of gradual lineage replacement across eastern China. This prediction is supported by initial field observations of FEAU expansion in a plateau lake (Li et al., 2026), but decadal monitoring and dispersal constraints are needed for validation.

bioRxiv preprint doi: https://doi.org/10.64898/2026.06.02.729718; this version posted June 8, 2026. The copyright holder for this preprint (which was not certified by peer review) is the author/funder, who has granted bioRxiv a license to display the preprint in perpetuity. It is made available under a CC-BY 4.0 International license.

530 Incorporating evolutionary history and functional genetic identity into ecological forecasting
531 remains essential as climate change reshapes ecosystems.

532 **Acknowledgments**

533 This work was supported by the National Natural Science Foundation of China (No. 32470388;
534 U22A20558; 32301317), Shandong Provincial Natural Science Foundation (ZR2024QC197),
535 and Tang Scholar Program. The authors thank Professor Jianquan Liu from Lanzhou University
536 and Dr. Kristin Saltonstall from the Smithsonian Tropical Research Institute for providing the
537 geographic information of the known haplotypes.

538 **Open Research Statement**

539 The raw sequence read data were submitted to the NCBI Sequence Read Archive with the
540 BioProject ID of PRJNA1126092. Data and code are available on Zenodo at
541 https://doi.org/10.5281/zenodo.20362090.

542 **Author Contributions**

543 L.L. (Lele Liu) led the conceptualization, investigation, methodology, validation, visualization,
544 and writing of the original draft. L.L. also contributed equally to formal analysis and acquired
545 funding. W.S. contributed equally to formal analysis and writing – review & editing, with
546 supporting efforts in investigation. Y.W. contributed equally to conceptualization and funding
547 acquisition, and led the writing – review & editing, with supporting roles in formal analysis and
548 investigation. L.L. (Lele Lin) contributed to conceptualization, funding acquisition,
549 investigation, and writing – review & editing. C.W. contributed to conceptualization,
550 methodology, visualization, and writing – review & editing. H.S. contributed to
551 conceptualization, funding acquisition, investigation, and writing – review & editing. Y.G.
552 contributed equally to writing – review & editing, with supporting roles in investigation,

bioRxiv preprint doi: https://doi.org/10.64898/2026.06.02.729718; this version posted June 8, 2026. The copyright holder for this preprint (which was not certified by peer review) is the author/funder, who has granted bioRxiv a license to display the preprint in perpetuity. It is made available under a CC-BY 4.0 International license.

553 methodology, and visualization. W.G. contributed equally to conceptualization, funding
554 acquisition, and writing – review & editing, and provided overall supervision for the project. All
555 authors reviewed and approved the final manuscript.

556 **Conflict of Interest Statement**

557 The authors declare no competing interests.

558 **References**

559 An, J., Wang, Q., Yang, J., & Liu, J. (2012). Phylogeographic analyses of *Phragmites australis*
560 in China: Native distribution and habitat preference of the haplotype that invaded North
561 America. *Journal of Systematics and Evolution, 3.544*, *50*(4), 334～340.
562 https://doi.org/10.1111/j.1759-6831.2012.00192.x

563 Bartolić, P., Morgan, E. J., Padilla-García, N., & Kolář, F. (2024). Ploidy as a leaky reproductive
564 barrier: Mechanisms, rates and evolutionary significance of interploidy gene flow. *Annals*
565 *of Botany*, *134*(4), 537～550. https://doi.org/10.1093/aob/mcae096

566 Breshears, D., Fontaine, J., Ruthrof, K., Field, J., Feng, X., Burger, J., Law, D., Kala, J., &
567 Hardy, G. (2021). Underappreciated plant vulnerabilities to heat waves. *New Phytologist*,
568 *231*(1), 32～39. https://doi.org/10.1111/nph.17348

569 Brix, H., Ye, S., Laws, E. A., Sun, D., Li, G., Ding, X., Yuan, H., Zhao, G., Wang, J., & Pei, S.
570 (2014). Large-scale management of common reed, *Phragmites australis*, for paper
571 production: A case study from the Liaohe Delta, China. *Ecological Engineering*, *73*, 760
572 ～769. https://doi.org/10.1016/j.ecoleng.2014.09.099

bioRxiv preprint doi: https://doi.org/10.64898/2026.06.02.729718; this version posted June 8, 2026. The copyright holder for this preprint (which was not certified by peer review) is the author/funder, who has granted bioRxiv a license to display the preprint in perpetuity. It is made available under a CC-BY 4.0 International license.

573 Brodie, J., Freeman, B., Mannion, P., & Hargreaves, A. (2025). Shifting, expanding, or
574 contracting? Range movement consequences for biodiversity. *Trends in Ecology &*
575 *Evolution*, *40*(5), 439～448. https://doi.org/10.1016/j.tree.2025.02.001
576 Bureš, P., Elliott, T., Veselý, P., Šmarda, P., Forest, F., Leitch, I., Nic Lughadha, E., Soto
577 Gomez, M., Pironon, S., Brown, M., Šmerda, J., & Zedek, F. (2024). The global
578 distribution of angiosperm genome size is shaped by climate. *New Phytologist*, *242*(2),
579 744～759. https://doi.org/10.1111/nph.19544
580 Chardon, N., Pironon, S., Peterson, M., & Doak, D. (2020). Incorporating intraspecific variation
581 into species distribution models improves distribution predictions, but cannot predict
582 species traits for a wide-spread plant species. *Ecography, 6.802*, *43*(1), 60～74.
583 https://doi.org/10.1111/ecog.04630
584 Chen, C., Liang, S., He, P., Liu, S., Wang, X., & Hu, Q. (1993). Chromosome counting in root-
585 tip cells of reed. *Journal of Shenyang Agricultural University*, *24*(2), 89～94.
586 Chen, K., Ye, H., Gu, L., Chen, J., & Li, G. (1993). Chromosome ability and mutagenic effect in
587 cell culture of *Phragmites communis*. *Chinese Bulletin of Botany*, *10*(1), 40～42.
588 Cheng, J., Li, J., Zhang, Z., Lu, H., Chen, G., Yao, B., Dong, Y., Ma, L., Yuan, X., Xu, J.,
589 Zhang, Y., Dai, W., Yang, X., Xue, L., Zhang, Y., Zhang, C., Mauricio, R., Peng, G., Hu,
590 S., Valverde B., Song X., Li Y., Stift M., & Qiang, S. (2021). Autopolyploidy-driven
591 range expansion of a temperate-originated plant to pan-tropic under global change.
592 *Ecological Monographs*, *91*(2), e01445. https://doi.org/10.1002/ecm.1445

bioRxiv preprint doi: https://doi.org/10.64898/2026.06.02.729718; this version posted June 8, 2026. The copyright holder for this preprint (which was not certified by peer review) is the author/funder, who has granted bioRxiv a license to display the preprint in perpetuity. It is made available under a CC-BY 4.0 International license.

593 Clark, L. V., & Jasieniuk, M. (2011). polysat: An R package for polyploid microsatellite
594 analysis. *Molecular Ecology Resources, 8.678*, *11*(3), 562～566.
595 https://doi.org/10.1111/j.1755-0998.2011.02985.x
596 Cui, X., Li, C., Qin, S., Huang, Z., Gan, B., Jiang, Z., Huang, X., Yang, X., Li, Q., Xiang, X.,
597 Chen, J., Zhao, Y., & Rong, J. (2022). High-throughput sequencing-based microsatellite
598 genotyping for polyploids to resolve allele dosage uncertainty and improve analyses of
599 genetic diversity, structure and differentiation: A case study of the hexaploid Camellia
600 oleifera. *Molecular Ecology Resources, 8.678*, *22*(1), 199～211.
601 https://doi.org/10.1111/1755-0998.13469
602 Di Cola, V., Broennimann, O., Petitpierre, B., Breiner, F. T., D'Amen, M., Randin, C., Engler,
603 R., Pottier, J., Pio, D., Dubuis, A., Pellissier, L., Mateo, R. G., Hordijk, W., Salamin, N.,
604 & Guisan, A. (2017). ecospat: An R package to support spatial analyses and modeling of
605 species niches and distributions. *Ecography*, *40*(6), 774～787.
606 https://doi.org/10.1111/ecog.02671
607 DuBois, K., Pollard, K., Kauffman, B., Williams, S., & Stachowicz, J. (2022). Local adaptation
608 in a marine foundation species: Implications for resilience to future global change.
609 *Global Change Biology, 13.211*, *28*(8), 2596～2610. https://doi.org/10.1111/gcb.16080
610 Earl, D., & vonHoldt, B. (2012). STRUCTURE HARVESTER: A website and program for
611 visualizing STRUCTURE output and implementing the Evanno method. *Conservation*
612 *Genetics Resources, 0.991*, *4*(2), 359～361. https://doi.org/10.1007/s12686-011-9548-7
613 Eller, F., Skálová, H., Caplan, J., Bhattarai, G., Burger, M., Cronin, J., Guo, W., Guo, X.,
614 Hazelton, E., Kettenring, K., Lambertini, C., McCormick, M., Meyerson, L., Mozdzer,

bioRxiv preprint doi: https://doi.org/10.64898/2026.06.02.729718; this version posted June 8, 2026. The copyright holder for this preprint (which was not certified by peer review) is the author/funder, who has granted bioRxiv a license to display the preprint in perpetuity. It is made available under a CC-BY 4.0 International license.

615 T., Pyšek, P., Sorrell, B., Whigham, D., & Brix, H. (2017). Cosmopolitan species as
616 models for ecophysiological responses to global change: The common reed *Phragmites*
617 *australis*. *Frontiers in Plant Science, 6.627*, *8*, 1833.
618 https://doi.org/10.3389/fpls.2017.01833
619 Exposito-Alonso, M., Booker, T., Czech, L., Gillespie, L., Hateley, S., Kyriazis, C., Lang, P.,
620 Leventhal, L., Nogues-Bravo, D., Pagowski, V., Ruffley, M., Spence, J., Toro Arana, S.,
621 Weiß, C., & Zess, E. (2022). Genetic diversity loss in the Anthropocene. *Science*,
622 *377*(6613), 1431～1435. https://doi.org/10.1126/science.abn5642
623 Fick, S., & Hijmans, R. (2017). WorldClim 2: New 1-km spatial resolution climate surfaces for
624 global land areas. *International Journal of Climatology*, *37*(12), 4302～4315.
625 https://doi.org/10.1002/joc.5086
626 Gou, X., Shi, H., Yu, S., Wang, Z., Li, C., Liu, S., Ma, J., Chen, G., Liu, T., & Liu, Y. (2020).
627 SSRMMD: A rapid and accurate algorithm for mining SSR feature loci and candidate
628 polymorphic SSRs based on assembled sequences. *Frontiers in Genetics*, *11*.
629 https://www.frontiersin.org/articles/10.3389/fgene.2020.00706
630 Guo, W., Cuda, J., Skalova, H., Lambertini, C., Pierce, S., Lucanova, M., Brix, H., Meyerson, L.,
631 & Pysek, P. (2024). Climate and genome size shape the intraspecific variation in
632 ecological adaptive strategies of a cosmopolitan grass species. *Functional Ecology*, *38*(9),
633 2054～2066. https://doi.org/10.1111/1365-2435.14613
634 Guo, W., Lambertini, C., Li, X., Meyerson, L., & Brix, H. (2013). Invasion of Old World
635 *Phragmites australis* in the New World: Precipitation and temperature patterns combined

bioRxiv preprint doi: https://doi.org/10.64898/2026.06.02.729718; this version posted June 8, 2026. The copyright holder for this preprint (which was not certified by peer review) is the author/funder, who has granted bioRxiv a license to display the preprint in perpetuity. It is made available under a CC-BY 4.0 International license.

636 with human influences redesign the invasive niche. *Global Change Biology, 13.211*,
637 *19*(11), 3406～3422. https://doi.org/10.1111/gcb.12295
638 Guo, X., Song, H., Wu, P., Liu, L., Li, M., Xie, L., Jespersen, E., Ye, S., & Guo, W. (2025).
639 Intraspecific variation in plant elementome reflects environment more than genetic and
640 epigenetic variation within a widespread grass (*Phragmites australis*). *Journal of Plant*
641 *Ecology*, rtaf070. https://doi.org/10.1093/jpe/rtaf070
642 Han, T., Wu, Q., Hou, X., Li, Z., Zou, Y., Ge, S., & Guo, Y. (2015). Frequent introgressions
643 from diploid species contribute to the adaptation of the tetraploid shepherd's purse
644 (Capsella bursa-pastoris). *Molecular Plant*, *8*(3), 427～438.
645 https://doi.org/10.1016/j.molp.2014.11.016
646 Jakobsson, M., & Rosenberg, N. A. (2007). CLUMPP: A cluster matching and permutation
647 program for dealing with label switching and multimodality in analysis of population
648 structure. *Bioinformatics (Oxford, England)*, *23*(14), 1801～1806.
649 https://doi.org/10.1093/bioinformatics/btm233
650 Kass, J., Pinilla-Buitrago, G., Paz, A., Johnson, B., Grisales-Betancur, V., Meenan, S., Attali, D.,
651 Broennimann, O., Galante, P., Maitner, B., Owens, H., Varela, S., Aiello-Lammens, M.,
652 Merow, C., Blair, M., & Anderson, R. (2023). wallace 2: A shiny app for modeling
653 species niches and distributions redesigned to facilitate expansion via module
654 contributions. *Ecography*, *2023*(3), e06547. https://doi.org/10.1111/ecog.06547
655 Kolář, F., Čertner, M., Suda, J., Schönswetter, P., & Husband, B. C. (2017). Mixed-ploidy
656 species: Progress and opportunities in polyploid research. *Trends in Plant Science,*
657 *22.012*, *22*(12), 1041～1055. https://doi.org/10.1016/j.tplants.2017.09.011

bioRxiv preprint doi: https://doi.org/10.64898/2026.06.02.729718; this version posted June 8, 2026. The copyright holder for this preprint (which was not certified by peer review) is the author/funder, who has granted bioRxiv a license to display the preprint in perpetuity. It is made available under a CC-BY 4.0 International license.

Lambertini, C., Guo, W., Ye, S., Eller, F., Guo, X., Li, X., Sorrell, B., Speranza, M., & Brix, H. (2020). Phylogenetic diversity shapes salt tolerance in *Phragmites australis* estuarine populations in East China. *Scientific Reports, 4.996*, *10*(1), 17645. https://doi.org/10.1038/s41598-020-74727-0

Lawlor, J., Comte, L., Grenouillet, G., Lenoir, J., Baecher, J. A., Bandara, R., Bertrand, R., Chen, I., Diamond, S., Lancaster, L., Moore, N., Murienne, J., Oliveira, B., Pecl, G., Pinsky, M., Rolland, J., Rubenstein, M., Scheffers, B., Thompson, L., van Amerom, B., Villalobos, F., Weiskopf, S., & Sunday, J. (2024). Mechanisms, detection and impacts of species redistributions under climate change. *Nature Reviews Earth & Environment*, *5*(5), 351～368. https://doi.org/10.1038/s43017-024-00527-z

Li, H. (2021). New strategies to improve minimap2 alignment accuracy. *Bioinformatics*, *37*(23), 4572～4574. https://doi.org/10.1093/bioinformatics/btab705

Li, W., Lin, L., Wang, Y., Sun, W., Guo, W., Bai, X., & Liu, L. (2026). Rapid expansion of the Eastern China lineage (haplotype P) of *Phragmites australis* in Caohai Lake, Guizhou, China. *Ecology and Evolution*, *16*(5), e73711. https://doi.org/10.1002/ece3.73711

Liu, L., Wang, J., Ma, X., Li, M., Guo, X., Yin, M., Cai, Y., Yu, X., Du, N., Wang, R., & Guo, W. (2021a). Impacts of the Yellow River and Qingtongxia dams on genetic diversity of *Phragmites australis* in Ningxia Plain, China. *Aquatic Botany, 1.968*, *169*, 103341. https://doi.org/10.1016/j.aquabot.2020.103341

Liu, L., Yin, M., Guo, X., Wang, J., Cai, Y., Wang, C., Yu, X., Du, N., Brix, H., Eller, F., Lambertini, C., & Guo, W. (2022). Cryptic lineages and potential introgression in a

bioRxiv preprint doi: https://doi.org/10.64898/2026.06.02.729718; this version posted June 8, 2026. The copyright holder for this preprint (which was not certified by peer review) is the author/funder, who has granted bioRxiv a license to display the preprint in perpetuity. It is made available under a CC-BY 4.0 International license.

679 mixed-ploidy species (*Phragmites australis*) across temperate China. *Journal of*
680 *Systematics and Evolution, 3.544*, *60*(2), 398～410. https://doi.org/10.1111/jse.12672
681 Liu, L., Yin, M., Guo, X., Yu, X., Song, H., Eller, F., Ma, X., Liu, X., Du, N., Wang, R., & Guo,
682 W. (2021b). The river shapes the genetic diversity of common reed in the Yellow River
683 Delta via hydrochory dispersal and habitat selection. *Science of The Total Environment,*
684 *10.753*, *764*, 144382. https://doi.org/10.1016/j.scitotenv.2020.144382
685 Liu, L., Yin, M., Guo, Y., Song, H., Guo, X., & Guo, W. (2026). Climatic adaptation and
686 phylogenetic history shape the intra-specific variation of CSR strategies in a widespread
687 grass. *Plant Diversity*, *48*(1), 181～191. https://doi.org/10.1016/j.pld.2025.06.001
688 López-Jurado, J., Mateos-Naranjo, E., & Balao, F. (2019). Niche divergence and limits to
689 expansion in the high polyploid Dianthus broteri complex. *New Phytologist*, *222*(2), 1076
690 ～1087. https://doi.org/10.1111/nph.15663
691 Meyerson, L., Cronin, J., Packer, J., Pyšek, P., & Saltonstall, K. (2025). Ecology, evolution, and
692 north american invasion of one of the world's most successful plant species. *Annual*
693 *Review of Ecology, Evolution, and Systematics*, *56*(1), 73～98.
694 https://doi.org/10.1146/annurev-ecolsys-102723-051221
695 Meyerson, L., Cronin, J., & Pyšek, P. (2016). *Phragmites australis* as a model organism for
696 studying plant invasions. *Biological Invasions*, *18*(9), 2421～2431.
697 https://doi.org/10.1007/s10530-016-1132-3
698 Pastore, A., Barabás, G., Bimler, M., Mayfield, M., & Miller, T. (2021). The evolution of niche
699 overlap and competitive differences. *Nature Ecology & Evolution*, *5*(3), 330～337.
700 https://doi.org/10.1038/s41559-020-01383-y

bioRxiv preprint doi: https://doi.org/10.64898/2026.06.02.729718; this version posted June 8, 2026. The copyright holder for this preprint (which was not certified by peer review) is the author/funder, who has granted bioRxiv a license to display the preprint in perpetuity. It is made available under a CC-BY 4.0 International license.

Paudel, R., Fristoe, T., Kinlock, N., Davis, A., Zhao, W., Van Calster, H., Chytrý, M., Danihelka, J., Decocq, G., Ehrendorfer - Schratt, L., Guo, K., Guo, W., Kaplan, Z., Pierce, S., Wild, J., Dawson, W., Essl, F., Kreft, H., Pergl, J., Pysek, P., Winter, M., & van Kleunen, M. (2025). Many plants naturalized as aliens abroad have also become more common within their native regions. *Nature Communications*, *16*(1), 8227. https://doi.org/10.1038/s41467-025-63293-6

Perez, T., Socha, A., Tserej, O., & Feeley, K. (2021). Photosystem II heat tolerances characterize thermal generalists and the upper limit of carbon assimilation. *Plant, Cell & Environment*, *44*(7), 2321～2330. https://doi.org/10.1111/pce.13990

Phillips, S., Anderson, R., Dudík, M., Schapire, R., & Blair, M. (2017). Opening the black box: An open-source release of Maxent. *Ecography*, *40*(7), 887～893. https://doi.org/10.1111/ecog.03049

Pritchard, J., Stephens, M., & Donnelly, P. (2000). Inference of population structure using multilocus genotype data. *Genetics, 4.402*, *155*(2), 945～959.

Pyšek, P., Skálová, H., Čuda, J., Guo, W., Suda, J., Doležal, J., Kauzál, O., Lambertini, C., Lučanová, M., Mandáková, T., Moravcová, L., Pyšková, K., Brix, H., & Meyerson, L. (2018). Small genome separates native and invasive populations in an ecologically important cosmopolitan grass. *Ecology*, *99*(1), 79～90. https://doi.org/10.1002/ecy.2068

Qiao, X., Zhang, J., Wang, Z., Xu, Y., Zhou, T., Mi, X., Cao, M., Ye, W., Jin, G., Hao, Z., Wang, X., Wang, X., Tian, S., Li, X., Xiang, W., Liu, Y., Shao, Y., Xu, K., Sang, W., Zeng F., Ren H., Jiang M., & Ellison, A. (2021). Foundation species across a latitudinal gradient in China. *Ecology*, *102*(2), e03234. https://doi.org/10.1002/ecy.3234

bioRxiv preprint doi: https://doi.org/10.64898/2026.06.02.729718; this version posted June 8, 2026. The copyright holder for this preprint (which was not certified by peer review) is the author/funder, who has granted bioRxiv a license to display the preprint in perpetuity. It is made available under a CC-BY 4.0 International license.

723 Qiu, J., Zhang, J., Wang, Y., & Zhuang, H. (2024). PPDC: An online platform for the prediction
724 of plant distributions in China. *Journal of Plant Ecology*, *17*(6), rtae094.
725 https://doi.org/10.1093/jpe/rtae094
726 Ran, J., Meng, B., Zhang, X., Huang, X., & Tu, S. (2025). Effect of reed expansion on habitat
727 adaptation and behavioral activity characteristics of grus nigricollis in Guizhou Caohai
728 National Nature Reserve. *Chinese Journal of Wildlife*, *46*(1), 107～117.
729 https://doi.org/10.12375/ysdwxb.20250112
730 Saltonstall, K. (2002). Cryptic invasion by a non-native genotype of the common reed,
731 *Phragmites australis*, into North America. *Proceedings of the National Academy of*
732 *Sciences*, *99*(4), 2445～2449. https://doi.org/10.1073/pnas.032477999
733 Saltonstall, K. (2003). Microsatellite variation within and among North American lineages of
734 *Phragmites australis*. *Molecular Ecology, 6.622*, *12*(7), 1689～1702.
735 https://doi.org/10.1046/j.1365-294X.2003.01849.x
736 Séférian, R., Nabat, P., Michou, M., Saint-Martin, D., Voldoire, A., Colin, J., Decharme, B.,
737 Delire, C., Berthet, S., Chevallier, M., Sénési, S., Franchisteguy, L., Vial, J., Mallet, M.,
738 Joetzjer, E., Geoffroy, O., Guérémy, J., Moine, M., Msadek, R., Ribes, A., Rocher, M.,
739 Roehrig, R., Salas-y-Mélia, D., Sanchez, E., Terray, L., Valcke, S., Waldman, R.,
740 Aumont, O., Bopp, L., Deshayes, J., Éthé, C., & Madec, G. (2019). Evaluation of CNRM
741 Earth System Model, CNRM-ESM2-1: role of Earth System processes in present-day and
742 future climate. *Journal of Advances in Modeling Earth Systems*, *11*(12), 4182～4227.
743 https://doi.org/10.1029/2019MS001791

bioRxiv preprint doi: https://doi.org/10.64898/2026.06.02.729718; this version posted June 8, 2026. The copyright holder for this preprint (which was not certified by peer review) is the author/funder, who has granted bioRxiv a license to display the preprint in perpetuity. It is made available under a CC-BY 4.0 International license.

744 Song, H., Jespersen, E., Guo, X., Du, N., Xie, L., Pei, L., Ye, S., Wang, R., Brix, H., Eller, F., &
745 Guo, W. (2021). Differences in relative air humidity affect responses to soil salinity in
746 freshwater and salt marsh populations of the dominant grass species *Phragmites*
747 *australis*. *Hydrobiologia, 2.822*, *848*(14), 3353～3369. https://doi.org/10.1007/s10750-
748 020-04285-z
749 Suarez-Gonzalez, A., Lexer, C., & Cronk, Q. (2018). Adaptive introgression: A plant
750 perspective. *Biology Letters*, *14*(3), 20170688. https://doi.org/10.1098/rsbl.2017.0688
751 Tanaka, T., Irbis, C., & Inamura, T. (2017). Phylogenetic analyses of *Phragmites* spp. In
752 southwest China identified two lineages and their hybrids. *Plant Systematics and*
753 *Evolution, 1.644*, *303*(6), 699～707. https://doi.org/10.1007/s00606-017-1403-1
754 Van de Peer, Y., Mizrachi, E., & Marchal, K. (2017). The evolutionary significance of
755 polyploidy. *Nature Reviews. Genetics*, *18*(7), 411～424.
756 https://doi.org/10.1038/nrg.2017.26
757 Vranken, S., Wernberg, T., Scheben, A., Severn-Ellis, A., Batley, J., Bayer, P., Edwards, D.,
758 Wheeler, D., & Coleman, M. (2021). Genotype–Environment mismatch of kelp forests
759 under climate change. *Molecular Ecology*, *30*(15), 3730～3746.
760 https://doi.org/10.1111/mec.15993
761 Wang, C., Liu, L., Yin, M., Eller, F., Brix, H., Wang, T., Salojärvi, J., & Guo, W. (2024).
762 Genome-wide analysis tracks the emergence of intraspecific polyploids in *Phragmites*
763 *australis*. *Npj Biodiversity*, *3*(1), 1～15. https://doi.org/10.1038/s44185-024-00060-8
764 Wang, C., Liu, L., Yin, M., Liu, B., Wu, Y., Eller, F., Gao, Y., Brix, H., Wang, T., Guo, W., &
765 Salojärvi, J. (2024). Chromosome-level genome assemblies reveal genome evolution of

bioRxiv preprint doi: https://doi.org/10.64898/2026.06.02.729718; this version posted June 8, 2026. The copyright holder for this preprint (which was not certified by peer review) is the author/funder, who has granted bioRxiv a license to display the preprint in perpetuity. It is made available under a CC-BY 4.0 International license.

766 an invasive plant *Phragmites australis*. *Communications Biology*, *7*(1), 1～14.
767 https://doi.org/10.1038/s42003-024-06660-1
768 Wang, C., Ord, J., Yan, M., Cai, Y., Shao, H., Lin, L., Salojärvi, J., Liu, L., & Guo, W. (2026).
769 Single-cell and spatial transcriptomics in *Phragmites australis* reveal the association of B
770 chromosomes with plant invasiveness. *Genome Biology*. https://doi.org/10.1186/s13059-
771 026-04079-x
772 Wang, C., Wang, T., Yin, M., Eller, F., Liu, L., Brix, H., & Guo, W. (2021). Transcriptome
773 analysis of tetraploid and octoploid common reed (*Phragmites australis*). *Frontiers in*
774 *Plant Science, 6.627*, *12*, 746. https://doi.org/10.3389/fpls.2021.653183
775 Wei, J., Han, W., Wang, W., Zhang, L., & Rajagopalan, B. (2023). Intensification of heatwaves
776 in China in recent decades: Roles of climate modes. *Npj Climate and Atmospheric*
777 *Science*, *6*(1), 98. https://doi.org/10.1038/s41612-023-00428-w
778 Wei, N., Du, Z., Liston, A., & Ashman, T. (2020). Genome duplication effects on functional
779 traits and fitness are genetic context and species dependent: Studies of synthetic
780 polyploid *Fragaria*. *American Journal of Botany*, *107*(2), 262～272.
781 https://doi.org/10.1002/ajb2.1377
782 Yan, J., Zhang, Y., Crawford, K., Chen, X., Yu, S., & Wu, J. (2021). Plant genotypic diversity
783 effects on soil nematodes vary with trophic level. *New Phytologist, 10.323*, *229*(1), 575～
784 584. https://doi.org/10.1111/nph.16829
785 Yin, M., Zhang, X., Zhu, H., Sheng, W., Wu, Y., Jiang, D., Wen, Q., Shao, H., Guo, Y., Wang,
786 C., Ma, L., Yu, X., Brix, H., Liu, L., & Guo, W. (2024). Trade-offs between Cd
787 bioconcentration and translocation and underlying physiological and rhizobacterial

bioRxiv preprint doi: https://doi.org/10.64898/2026.06.02.729718; this version posted June 8, 2026. The copyright holder for this preprint (which was not certified by peer review) is the author/funder, who has granted bioRxiv a license to display the preprint in perpetuity. It is made available under a CC-BY 4.0 International license.

788 mechanisms in *Phragmites australis*. *Journal of Environmental Management*, *371*,
789 123291. https://doi.org/10.1016/j.jenvman.2024.123291
790 Zhang, L., Van Riemsdijk, I., Liu, M., Liao, Z., Cavé-Radet, A., Bi, J., Wang, S., Zhao, Y., Cao,
791 P., Parepa, M., Bossdorf, O., Salmon, A., Aïnouche, M., Ju, R., Wu, J., Richards, C., &
792 Li, B. (2024). Biogeography of a global plant invader: From the evolutionary history to
793 future distributions. *Global Change Biology*, *30*(12), e17622.
794 https://doi.org/10.1111/gcb.17622
795 Zhao, Y., Wang, S., Liao, Z., Parepa, M., Zhang, L., Cao, P., Bi, J., Guo, Y., Bossdorf, O.,
796 Richards, C. L., Wu, J., Li, B., & Ju, R. (2024). Geographic variation in leaf traits and
797 palatability of a native plant invader during domestic expansion. *Ecology*, *105*(11),
798 e4425. https://doi.org/10.1002/ecy.4425
799 Zhou, J., Zhao, J., Li, Y., Bai, Y., Wu, Y., Xiang, B., & Zhu, H. (2024). The hottest center:
800 Characteristics of high temperatures in midsummer of 2022 in Chongqing and its
801 comparison with 2006. *Theoretical and Applied Climatology*, *155*(1), 151～162.
802 https://doi.org/10.1007/s00704-023-04609-8
803 Zohren, J., Wang, N., Kardailsky, I., Borrell, J., Joecker, A., Nichols, R., & Buggs, R. (2016).
804 Unidirectional diploid–tetraploid introgression among British birch trees with shifting
805 ranges shown by restriction site-associated markers. *Molecular Ecology*, *25*(11), 2413～
806 2426. https://doi.org/10.1111/mec.13644

bioRxiv preprint doi: https://doi.org/10.64898/2026.06.02.729718; this version posted June 8, 2026. The copyright holder for this preprint (which was not certified by peer review) is the author/funder, who has granted bioRxiv a license to display the preprint in perpetuity. It is made available under a CC-BY 4.0 International license.

Figures

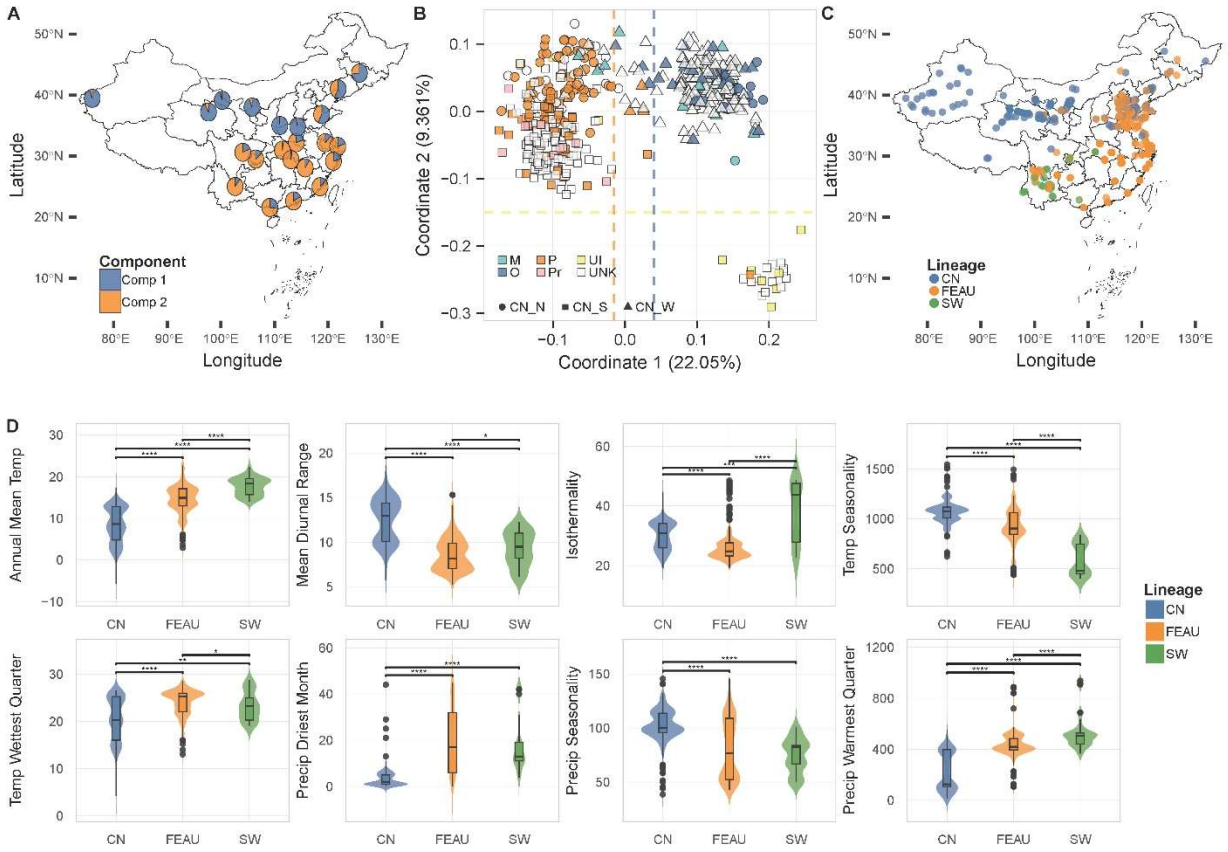


Figure 1 Evolutionary lineages of *Phragmites australis* in China. **(A)** Bayesian clustering analysis based on 42 nuclear microsatellites at the optimal genetic cluster number $K = 2$. **(B)** Principal coordinate analysis (PCoA) based on Bruvo's genetic distance. Colors indicate chloroplast haplotypes, where P_r denotes P-related haplotypes and "Unknown" refers to samples without haplotype data. Shapes denote geographical origins: circles (northern China, CN_N), squares (southern China, CN_S), and triangles (northwestern China, CN_W). **(C)** Geographical distribution of sampling locations for each genetic lineage by PCoA or/and chloroplast haplotypes. **(D)** Bioclimatic variable differences among lineages. Bio1, annual mean temperature; bio2, mean diurnal range; bio3, isothermality; bio4, temperature seasonality; bio8, mean temperature of wettest quarter; bio14, precipitation of driest month; bio15, precipitation seasonality; bio18, precipitation of warmest quarter. Significance levels are indicated as: * $p < 0.05$, ** $p < 0.01$, *** $p < 0.001$.

bioRxiv preprint doi: https://doi.org/10.64898/2026.06.02.729718; this version posted June 8, 2026. The copyright holder for this preprint (which was not certified by peer review) is the author/funder, who has granted bioRxiv a license to display the preprint in perpetuity. It is made available under a CC-BY 4.0 International license.

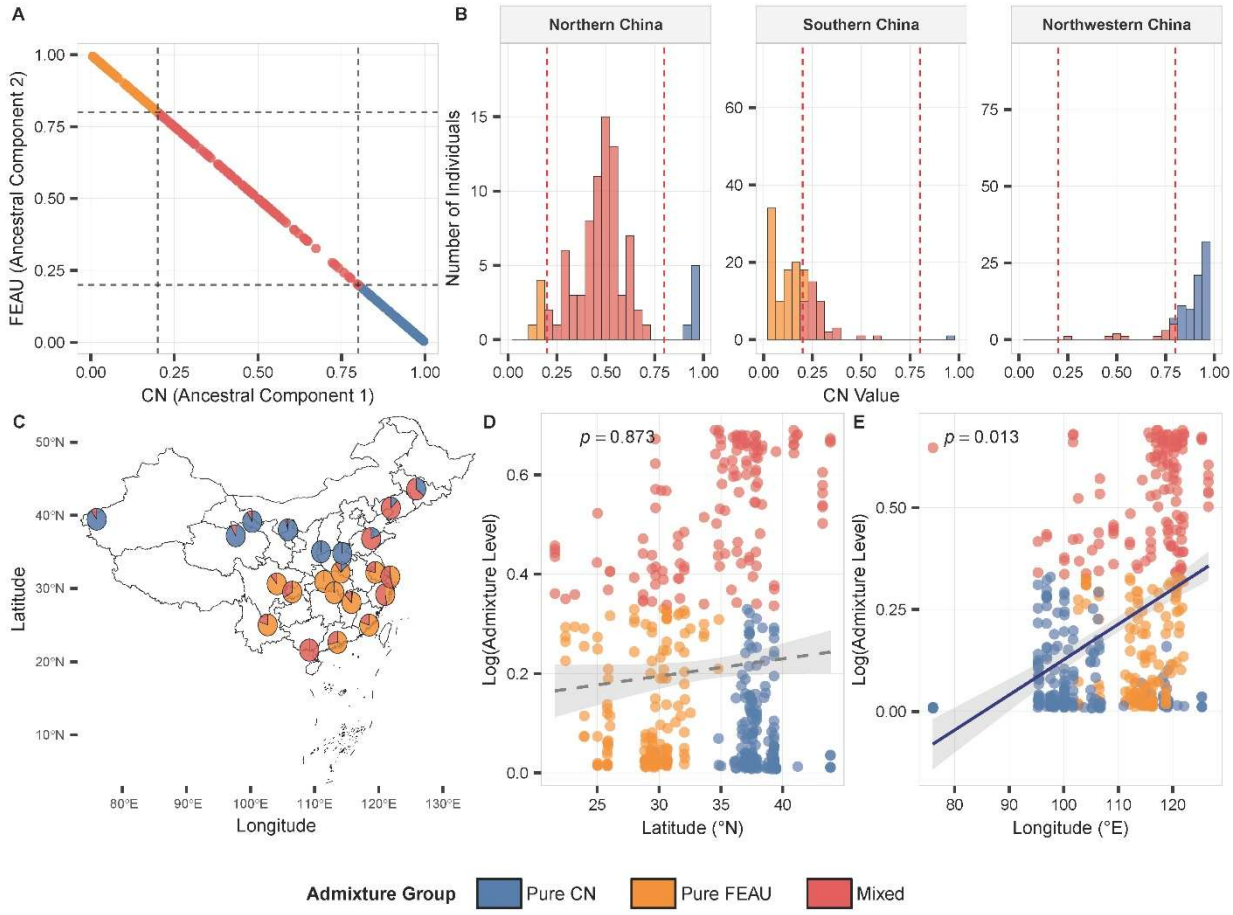


Figure 2 Admixture and introgression between CN and FEAU lineages revealed by STRUCTURE. **(A)** Scatter plot of individual ancestry coefficients for the two ancestral components (CN and FEAU). Dashed lines indicate the 0.2 and 0.8 thresholds used to define pure and admixed individuals. Points are colored by admixture group. STRUCTURE is used here to detect hybridization, not to define lineages (see Figure 1). **(B)** Histograms of CN ancestry values across three geographic regions: Northern China, Southern China, and Northwestern China. **(C)** Geographic distribution of admixture groups across Chinese provinces. Pie charts show the relative proportions of pure CN (blue), pure FEAU (orange), and mixed (red) individuals in each province. **(D)** Relationship between latitude and log-transformed admixture level. Points are colored by admixture group. The regression line (solid if $p < 0.05$, dashed if $p > 0.05$) and p-value (from linear mixed-effects model with Province as random effect) are shown. The admixture level for each individual was calculated as $1 - 2 \times |CN - 0.5|$, where CN is the ancestry coefficient of the CN lineage (range 0 - 1). This value approaches 1 when CN = 0.5

bioRxiv preprint doi: https://doi.org/10.64898/2026.06.02.729718; this version posted June 8, 2026. The copyright holder for this preprint (which was not certified by peer review) is the author/funder, who has granted bioRxiv a license to display the preprint in perpetuity. It is made available under a CC-BY 4.0 International license.

(high admixture) and approaches 0 when CN is near 0 or 1 (near-pure ancestry). To improve visualization, we plotted log (admixture level + 1), which ranges from 0 (pure) to log (2) ≈ 0.69 (maximally admixed). **(E)** Relationship between longitude and log-transformed admixture level. Visualization follows the same conventions as panel D. Pure individuals are defined as having > 80% ancestry from one component; individuals with 20-80% ancestry from each component are classified as mixed.

bioRxiv preprint doi: https://doi.org/10.64898/2026.06.02.729718; this version posted June 8, 2026. The copyright holder for this preprint (which was not certified by peer review) is the author/funder, who has granted bioRxiv a license to display the preprint in perpetuity. It is made available under a CC-BY 4.0 International license.

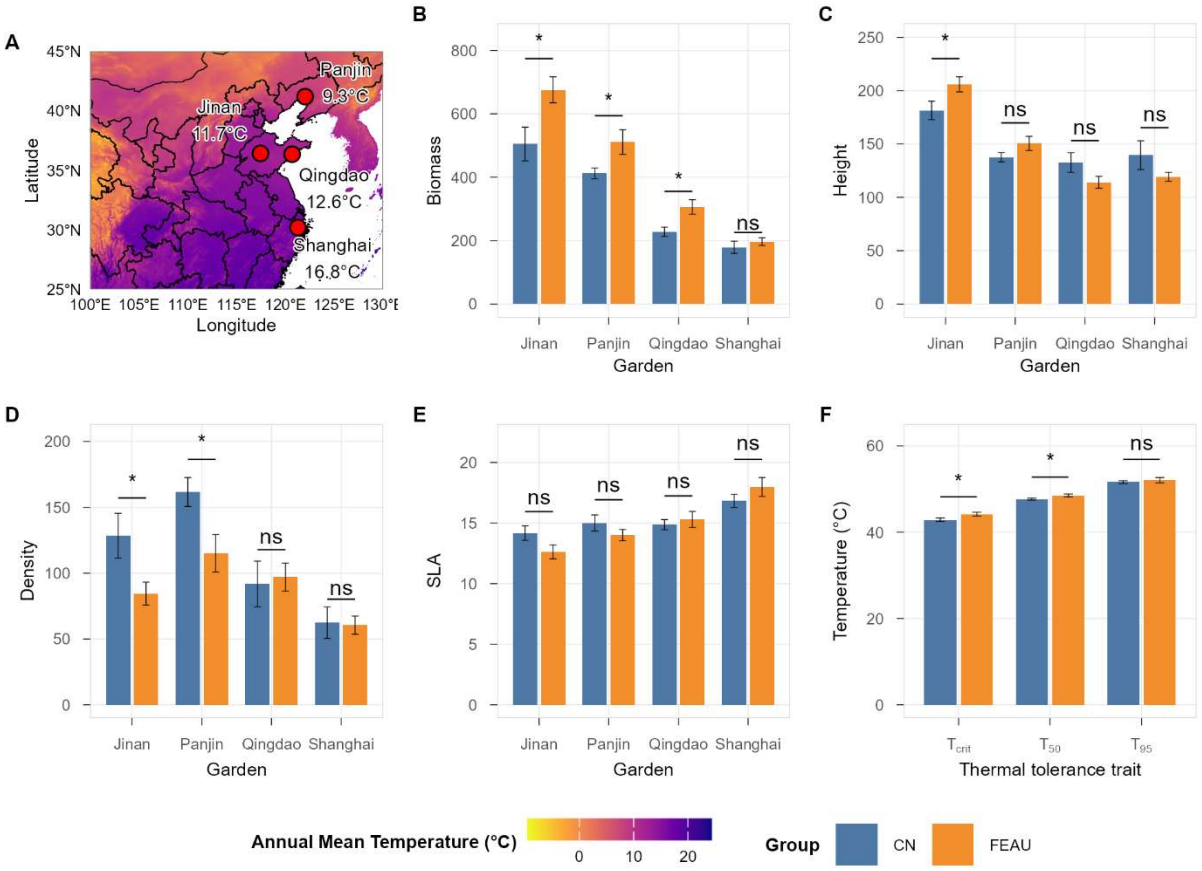


Figure 3 Comparative growth performance and heat tolerance of the CN and FEAU lineages of *Phragmites australis* across common garden environments. **(A)** Geographic locations of the four common garden sites (Panjin, Jinan, Qingdao, Shanghai) overlaid on the mean annual temperature (Bio1) raster map of eastern China. Color gradient represents annual mean temperature (°C). **(B-E)** Comparison of four growth traits between lineages across four common garden locations: **(B)** Total Biomass, **(C)** Shoot Height, **(D)** Density, and **(E)** Specific Leaf Area (SLA). Bar heights represent mean values, and error bars indicate the standard error of the mean. **(F)** Comparison of key heat tolerance parameters (T_{crit}, T_{50} and T_{95}) between the CN and FEAU lineages. Significance levels from pairwise *t* tests within each garden **(B-E)** and unpraised *t* tests for heat tolerance parameters **(F)** are denoted by asterisks: * $p < 0.05$, ** $p < 0.01$, *** $p < 0.001$; "ns" indicates not significant.

bioRxiv preprint doi: https://doi.org/10.64898/2026.06.02.729718; this version posted June 8, 2026. The copyright holder for this preprint (which was not certified by peer review) is the author/funder, who has granted bioRxiv a license to display the preprint in perpetuity. It is made available under a CC-BY 4.0 International license.

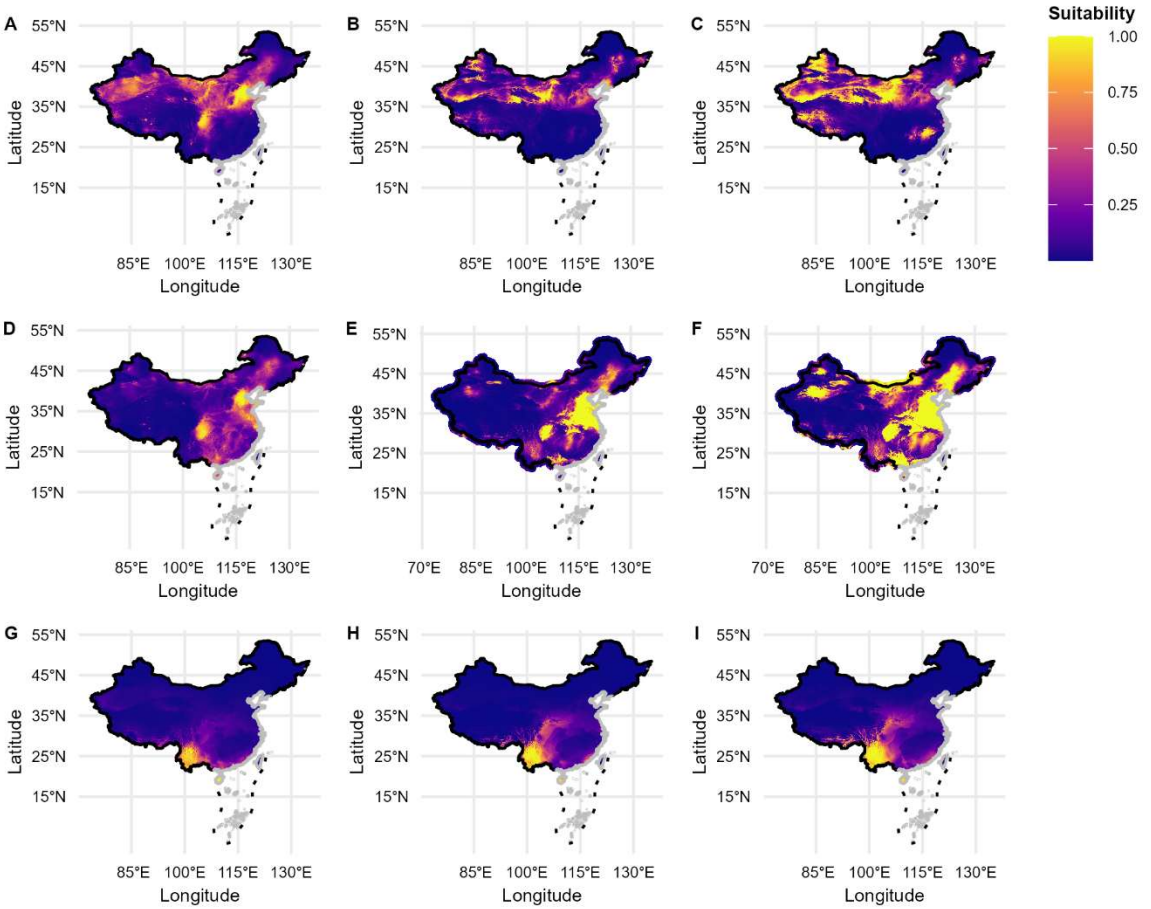


Figure 4 Predicted potential distribution of three *Phragmites australis* lineages (CN, FEAU, and SW) in China under current and future climate scenarios. The first row (A, B, C) shows the results for the CN lineage, the second row (D, E, F) for the FEAU lineage, and the third row (G, H, I) for the SW lineage. Columns represent different time periods: current distribution (A, D, G), and projected distributions for 2061–2080 under the low-emission scenario SSP1-2.6 (B, E, H) and the high-emission scenario SSP5-8.5 (C, F, I). Predictions were generated using the Maximum Entropy (MaxEnt) model. The depth of color (color intensity) corresponds to the level of habitat suitability, ranging from dark blue (unsuitable) to bright yellow (highly suitable).